

Article

Global Dynamics for Competition between Two *Wolbachia* Strains with Bidirectional Cytoplasmic Incompatibility

Qiming Huang, Lijie Chang, Zhaowang Zhang  and Bo Zheng * 

College of Mathematics and Information Sciences, Guangzhou University, Guangzhou 510006, China

* Correspondence: zhengbo611@outlook.com

Abstract: Releasing *Wolbachia*-infected mosquitoes to suppress or replace wild vector mosquitoes has been carried out in 24 countries worldwide, showing great promise in controlling mosquitoes and mosquito-borne diseases. To face the instability of *Wolbachia* infection in different environments during the area-wide application, we should consider the overlapping of two *Wolbachia* strains. In this case, bidirectional cytoplasmic incompatibility occurs, which results in mating partners infected with exclusive *Wolbachia* strains producing inviable offspring. To determine the better *Wolbachia* candidate for release, we develop an ordinary differential equation model to study the global dynamics for competition between two *Wolbachia* strains. Our theoretical results on the sharp estimate of stable curves completely determine the fate of the two *Wolbachia* strains, which help choose appropriate strains for release.

Keywords: mosquito-borne diseases; stable curve; planar system; stability analysis; complete or incomplete cytoplasmic incompatibility

MSC: 92B05; 37N25; 34D23; 92D30



Citation: Huang, Q.; Chang, L.; Zhang, Z.; Zheng, B. Global Dynamics for Competition between Two *Wolbachia* Strains with Bidirectional Cytoplasmic Incompatibility. *Mathematics* **2023**, *11*, 1691. <https://doi.org/10.3390/math11071691>

Academic Editors: Osman Tunç, Vitalii Slynko and Sandra Pinelas

Received: 22 February 2023

Revised: 28 March 2023

Accepted: 30 March 2023

Published: 1 April 2023



Copyright: © 2023 by the authors. Licensee MDPI, Basel, Switzerland. This article is an open access article distributed under the terms and conditions of the Creative Commons Attribution (CC BY) license (<https://creativecommons.org/licenses/by/4.0/>).

1. Introduction

With an estimated 700,000 deaths annually, vector-borne infections cause an overwhelming disease burden on humans [1]. Dengue fever is a mosquito-borne disease transmitted through bites of female *Aedes* mosquitoes, including *Aedes aegypti* and *Aedes albopictus* mosquitoes. More than half of the world's population is at risk of dengue [2,3]. The most direct method to combat dengue vectors is spraying insecticides to kill them, which has only short-term effects due to the appearance of insecticide resistance [4]. Meanwhile, the development of dengue vaccines is still at a difficult stage because of antibody-dependent enhancement (ADE) among the four serotypes of dengue viruses [5,6]. Several biological control methods have been implemented to deal with this situation, one of which involves the endosymbiotic bacteria *Wolbachia*.

Wolbachia are common and widespread intracellular bacteria of arthropods, which exist in more than 66% of all insect species [7], including some species of mosquitoes. *Wolbachia* were first identified in 1924 by Hertig and Wolbach [8]. In 1952, scientists found that *Wolbachia* in *Culex autogenicus* [9] caused unidirectional cytoplasmic incompatibility (CI for short): when *Wolbachia*-infected males mate with uninfected females, their offspring are not viable. Since then, *Wolbachia*-infected males that cause CI have been proposed as an innovative way to decrease vector populations. However, *Aedes aegypti* does not carry *Wolbachia*, and although *Aedes albopictus* naturally carries two kinds of *Wolbachia*, it does not induce CI. This situation halted the progress of the use of *Wolbachia* to combat dengue fever until 2005, by embryonic microinjection. The authors in [10] successfully established the first *Wolbachia* strain (*w*Ri) that causes CI in *Aedes aegypti*. Later in 2006 [11], they also established *w*AlbB in *Aedes albopictus* by transferring *Wolbachia* from *Drosophila simulans*. In addition to inducing CI, both *w*AlbB in *Aedes aegypti* and *w*Ri in *Aedes albopictus* are

completely maternally transmitted, that is, the offspring of *Wolbachia*-infected females are all infected [10,11]. Furthermore, both of them can block the replication of dengue viruses in mosquitoes. Hence, *Wolbachia*-infected males that induce CI can be regarded as a flying and resistance-free insecticide, and *Wolbachia*-infected females can block the transmission of dengue viruses between humans and mosquitoes.

Two *Wolbachia* release strategies have been proposed based on these observations. One is to only release *Wolbachia*-infected males to sterilize and suppress wild female mosquitoes; this is named population suppression. The other is usually termed population replacement, in which both *Wolbachia*-infected females and *Wolbachia*-infected males are released to replace the wild mosquito populations with *Wolbachia*-infected ones, so they have reduced or no capacity to transmit dengue viruses. The first field trial of population suppression was carried out from 2015 to 2017 in Guangzhou, China, which suppressed more than 90% of the wild-type *Aedes albopictus* field populations [12]. The first population replacement was implemented in 2009 in Cairns, Australia [13–15]. Since then, the *Wolbachia* infection frequency in mosquito populations has been kept high enough to make the release sites dengue-free areas. The success of population suppression and population replacement makes the *Wolbachia* release method a promising method to control mosquito and mosquito-borne diseases [16]. Nowadays, *Wolbachia* release has been carried out worldwide, including in Yogyakarta, Indonesia (2014) with nearly 100% *Wolbachia* coverage rate, and 77% reduction in dengue incidence, in Kuala Lumpur, Malaysia (2013) with 80% *Wolbachia* coverage rate, and 40% reduction in dengue incidence, and in Niteroi, Brazil (2014) with 40–80% *Wolbachia* coverage rate, and 69% reduction in dengue incidence.

As a biologically safe and environmentally friendly method, mathematical models aiming to analyze the interactive dynamics of the released and wild mosquitoes have been developed. We refer to [12,17–20] for models on population suppression, and [21–24] for models on population replacement, to cite a few. However, all the above models only include a single *Wolbachia* strain, which induces unidirectional CI. In this paper, we focus on the case of bidirectional CI, which results in the mating partners infected with mutually exclusive *Wolbachia* strains producing inviable offspring [25–27]. For example, in the host *Aedes albopictus*, the authors in [28] found bidirectional CI for crosses between ARwP and SR lines in *Aedes albopictus*. The egg hatch rate of the reciprocal crosses between ARwP and SR mosquitoes are 0, while almost 90% eggs hatch successfully from crosses ARwP × ARwP and SR × SR. Bidirectional CI has also been found in the species *Culex quinquefasciatus* carrying wPip and wAlbA [29], in the species *Porcellio dilatatus* carrying wPet and wDil [30], and in *Aedes aegypti* carrying three strains wAlbA, wAlbB, and wMel [31].

Another motivation driving us to study bidirectional CI is that for the area-wide application of *Wolbachia* release, we should take the overlapping of two *Wolbachia* strains into consideration, which could induce bidirectional CI. This consideration is based on mounting evidence showing that temperature and possibly other environmental and ecological conditions impact the maternal transmission rate and the CI intensity, and hence impact the potential of *Wolbachia* mosquitoes to invade populations and persist [32–35]. For example, in [32], the authors checked three *Wolbachia* strains, wMel, wMelPop-CLA, and wAlbB. They found that under cyclical temperatures of 26–37 °C, only wAlbB shows complete CI, while both wMel and wMelPop-CLA show incomplete CI. Regarding the maternal transmission efficiency, both wMel and wMelPop-CLA completely lose their maternal transmission ability when the maintenance temperature for offspring is 26–37 °C. Therefore, if the released *Wolbachia* mosquitoes lose their reproductive advantage to replace wild mosquitoes, another new *Wolbachia* strain should be supplemented to achieve the replacement.

2. Model Development

To model this, we denote the two mutually exclusive *Wolbachia* strains as *w-A* and *w-B*. Then only both parents harboring the same *Wolbachia* strains can produce viable offspring; otherwise, there will be no offspring due to complete CI. Let $I_A^E(t)$, $I_A^M(t)$, $I_B^E(t)$

and $I_B^M(t)$ be the numbers of w -A females, w -A males, w -B females, and w -B males at time t , respectively.

Denote the natural birth rate of w -A mosquitoes by b_A and that of w -B mosquitoes by b_B . Let $s_h^A \in (0, 1]$ be the proportion of unhatched eggs produced from the incompatible cross if the father carries with w -B. Therefore, s_h^A quantifies the intensity of CI of the incompatible mating between the w -A female and the w -B male [36,37]. Similarly, let $s_h^B \in (0, 1]$ be the CI intensity if the father is infected with w -A. Denote the density-dependent death rates for w -A mosquitoes and w -B mosquitoes by d_A and d_B , respectively. With the assumption of random mating behavior [38], the probability of I_A^F mating with I_A^M is $I_A^M / (I_A^M + I_B^M)$, and the probability mating with I_B^M is $I_B^M / (I_A^M + I_B^M)$. If we assume that the birth ratio of female to male is 1:1 [39], then the growth of I_A^F is

$$\frac{b_A}{2} \cdot I_A^F \cdot \left[\frac{I_A^M}{I_A^M + I_B^M} + (1 - s_h^A) \cdot \frac{I_B^M}{I_A^M + I_B^M} \right] = \frac{b_A}{2} \cdot I_A^F \cdot \left(1 - s_h^A \cdot \frac{I_B^M}{I_A^M + I_B^M} \right).$$

To investigate the density-dependent effect of all mosquitoes on w -A, we denote the total number of mosquitoes as

$$T(t) = I_A^F(t) + I_A^M(t) + I_B^F(t) + I_B^M(t).$$

Thus, we obtain the equation for I_A^F

$$\frac{dI_A^F(t)}{dt} = \frac{b_A}{2} \cdot I_A^F(t) \cdot \left(1 - s_h^A \cdot \frac{I_B^M(t)}{I_A^M(t) + I_B^M(t)} \right) - d_A T(t) I_A^F(t), \tag{1}$$

where $d_A T(t) I_A^F(t)$ denotes the density-dependent decay. Similarly, regarding I_A^M , I_B^F and I_B^M , we have the following equations:

$$\frac{dI_A^M(t)}{dt} = \frac{b_A}{2} \cdot I_A^F(t) \cdot \left(1 - s_h^A \cdot \frac{I_B^M(t)}{I_A^M(t) + I_B^M(t)} \right) - d_A T(t) I_A^M(t), \tag{2}$$

$$\frac{dI_B^F(t)}{dt} = \frac{b_B}{2} \cdot I_B^F(t) \cdot \left(1 - s_h^B \cdot \frac{I_A^M(t)}{I_A^M(t) + I_B^M(t)} \right) - d_B T(t) I_B^F(t), \tag{3}$$

$$\frac{dI_B^M(t)}{dt} = \frac{b_B}{2} \cdot I_B^F(t) \cdot \left(1 - s_h^B \cdot \frac{I_A^M(t)}{I_A^M(t) + I_B^M(t)} \right) - d_B T(t) I_B^M(t). \tag{4}$$

To help track the above equations, we refer the readers to Table 1 for the derivation of the first terms in Equations (1)–(4). The green and pink blocks are for the female offspring of w -A and w -B mosquitoes, respectively. The yellow blocks represent the loss due to CI.

Table 1. The wiring diagram for the derivation of the first terms in Equations (1)–(4).

| Matings | I_A^M | I_B^M |
|---------|--|--|
| I_A^F | $\frac{b_A}{2} \cdot I_A^F \cdot \frac{I_A^M}{I_A^M + I_B^M}$ | $\frac{b_A}{2} I_A^F (1 - s_h^A) \cdot \frac{I_B^M}{I_A^M + I_B^M}$ $\frac{b_A}{2} \cdot I_A^F \cdot s_h^A \cdot \frac{I_B^M}{I_A^M + I_B^M}$ |
| I_B^F | $\frac{b_B}{2} I_B^F (1 - s_h^B) \cdot \frac{I_A^M}{I_A^M + I_B^M}$ $\frac{b_B}{2} \cdot I_B^F \cdot s_h^B \cdot \frac{I_A^M}{I_A^M + I_B^M}$ | $\frac{b_B}{2} \cdot I_B^F \cdot \frac{I_B^M}{I_A^M + I_B^M}$ |

The assumption of equal sex determination for offspring [39] allows us to assume $I_A^F = I_A^M, I_B^F = I_B^M$. Let

$$x(t) = I_A^F(t) + I_A^M(t), y(t) = I_B^F(t) + I_B^M(t).$$

Then the four-dimensional System (1)–(4) is reduced to the planar system

$$\begin{aligned} \frac{dx}{dt} &= \frac{b_A}{2}x \left(1 - s_h^A \frac{y}{x+y} \right) - d_A x(x+y), \\ \frac{dy}{dt} &= \frac{b_B}{2}y \left(1 - s_h^B \frac{x}{x+y} \right) - d_B y(x+y). \end{aligned} \tag{5}$$

If we apply the rescaling

$$u = \frac{2d_B}{b_B}x, v = \frac{2d_B}{b_B}y, s = \frac{b_B}{2}t, \tag{6}$$

then the first equation in System (5) is transformed to

$$\begin{aligned} \frac{du}{ds} &= \frac{d\left(\frac{2d_B}{b_B}x\right)}{d\left(\frac{b_B}{2}t\right)} = \frac{4d_B}{b_B^2} \cdot \frac{dx}{dt} \\ &= \frac{4d_B}{b_B^2} \left(\frac{b_A}{2}x \left(1 - s_h^A \frac{y}{x+y} \right) - d_A x(x+y) \right) \\ &= \frac{4d_B}{b_B^2} \left(\frac{b_A}{2} \cdot \frac{b_B}{2d_B}u \left(1 - s_h^A \cdot \frac{v}{u+v} \right) - d_A \cdot \frac{b_B}{2d_B}u \cdot \frac{b_B}{2d_B}(u+v) \right) \\ &= \frac{b_A}{b_B}u \left(1 - s_h^A \cdot \frac{v}{u+v} \right) - \frac{d_A}{d_B}u(u+v). \end{aligned} \tag{7}$$

Applying the same process to the second equation in System (5), we can rescale System (5) as

$$\begin{aligned} \frac{du}{ds} &= \frac{4d_B}{b_B^2} \cdot \frac{dx}{dt} = \frac{b_A}{b_B}u \left(1 - s_h^A \frac{v}{u+v} \right) - \frac{d_A}{d_B}u(u+v), \\ \frac{dv}{ds} &= \frac{4d_B}{b_B^2} \cdot \frac{dy}{dt} = v \left(1 - s_h^B \frac{u}{u+v} \right) - v(u+v). \end{aligned} \tag{8}$$

Let $\beta = b_A/b_B$ and $\delta = d_A/d_B$, respectively, be the relative birth and death rates of w -A females to w -B females. By replacing u, v and s by x, y and t , System (8) becomes

$$\begin{aligned} \frac{dx}{dt} &= \beta x \left(1 - s_h^A \frac{y}{x+y} \right) - \delta x(x+y) := F(x,y), \\ \frac{dy}{dt} &= y \left(1 - s_h^B \frac{x}{x+y} \right) - y(x+y) := G(x,y). \end{aligned} \tag{9}$$

Remark 1. The rescaling (6) not only reduces the number of parameters from six to four but also makes the w -B mosquitoes stabilize at 1 without the interference of w -A mosquitoes. In such a situation, the value of $x(t)$ is not the absolute number of w -A mosquitoes. Instead, it estimates the proportion of w -A mosquitoes among all mosquitoes, which has been frequently used to record the Wolbachia infection frequency when studying the Wolbachia spread dynamics in mosquito populations [12,22–24,36–38,40–42].

The rest of this paper is organized as follows. In Section 3.1, we analyze the dynamics of System (9) with complete CI, that is, $s_h^A = s_h^B = 1$. In this case, System (9) admits four equilibria, and we offer a relatively sharp estimation of the stable curve of the only saddle. Section 3.2 is devoted to the case of incomplete CI, which has been frequently reported in *Wolbachia* hosts. The entire classification of the global dynamics of System (9) with incomplete CI is offered. Finally, in Section 4, we provide a survey on the theoretical results and numerical simulations for the competition outcome between two *Wolbachia* strains. Table 2 provides the glossary of notation for model development.

Table 2. The glossary of notation.

| Symbol | Definition | Unit |
|----------------------|--|--|
| $I_A^F(t)(I_A^M(t))$ | Number of <i>w-A</i> females (males) at time t | — |
| $I_B^F(t)(I_B^M(t))$ | Number of <i>w-B</i> females (males) at time t | — |
| $T(t)$ | Number of total mosquitoes at time t | — |
| $b_A(b_B)$ | Natural birth rate of <i>w-A</i> (<i>w-B</i>) mosquitoes | Per female per unit of time |
| $s_h^A(s_h^B)$ | Proportion of unhatched eggs produced from the incompatible cross if the father carries with <i>w-B</i> (<i>w-A</i>) | — |
| $d_A(d_B)$ | Density-dependent death rates for <i>w-A</i> (<i>w-B</i>) mosquitoes | Per (mosquito) ² per unit of time |
| $x(t)$ | Number of total <i>w-A</i> mosquitoes at time t | — |
| $y(t)$ | Number of total <i>w-B</i> mosquitoes at time t | — |
| β | b_A/b_B | — |
| δ | d_A/d_B | — |

3. Results

3.1. Complete CI with $s_h^A = s_h^B = 1$

Complete CI has been repeatedly observed. For example, the experiment for *wMelPop* in *Aedes aegypti* in [43] shows that no eggs hatched from more than 2500 embryos obtained from the incompatible mating. The *Wolbachia* strain *wAlbB* in *Culex quinquefasciatus* [29], and *wPip*, *wAlbA* and *wAlbB* in *Aedes albopictus* [44] also manifest complete CI. In this section, we study the dynamics of System (9) when both *w-A* and *w-B* induce complete CI, that is, $s_h^A = s_h^B = 1$. In this case, System (9) becomes

$$\begin{aligned} \frac{dx}{dt} &= \beta x \left(1 - \frac{y}{x+y} \right) - \delta x(x+y) := f(x,y), \\ \frac{dy}{dt} &= y \left(1 - \frac{x}{x+y} \right) - y(x+y) := g(x,y). \end{aligned} \tag{10}$$

By defining

$$f(0,0) = g(0,0) = 0, \tag{11}$$

we have $E_0 = (0,0)$ as a trivial equilibrium. The remediation (11) will be maintained in the following discussion without further mention. Relying on the technique of linearization in the classical context of nonlinear dynamics [45], we count the equilibria of system (10) and analyze their stability in the following theorem.

Theorem 1. System (10) has four equilibria in the first quadrant, $E_0 = (0,0)$, $E_1 = (\beta/\delta,0)$, $E_2 = (0,1)$, and $E^* = (x^*,y^*) = (\beta\delta/(\beta + \delta)^2, \beta^2/(\beta + \delta)^2)$. The origin E_0 is a source, E_1 and E_2 are sinks, and E^* is a saddle.

Proof. The calculation to get the existence of the equilibria is trivial, and we omit it here. With the help of the x -isocline $x = \delta/\beta(x+y)^2$ and the y -isocline $y = (x+y)^2$, in Figure 1A we plot the direction field of System (10). Furthermore, panel B locates the neighborhood D_0 of $(0,0)$ such that any solution of System (10) initiated from D_0 will eventually exit from D_0 . Hence, there exists an $\varepsilon > 0$ and

$$D_0 = \left\{ (x(t), y(t)) : x(t) \geq 0, y(t) \geq 0, x^2(t) + y^2(t) < \varepsilon^2 \right\},$$

such that if $E^* \notin D_0$, then any solutions of System (10) initiated from D_0 will eventually exit from D_0 , proving the instability of E_0 .

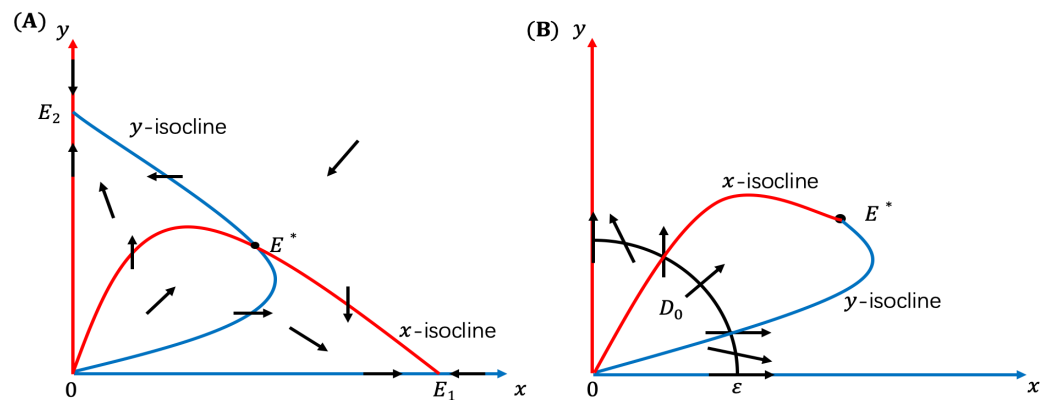


Figure 1. Panel (A) is for the direction field of System (10), and panel (B) spots an unstable neighborhood D_0 of $(0,0)$.

Regarding the local asymptotic stability of E_1 and E_2 , we calculate the Jacobian matrix of (10) at (x, y) as

$$\mathcal{J}(x, y) = \begin{pmatrix} \beta \left(1 - \frac{y^2}{(x+y)^2} \right) - \delta(2x+y) & -\beta \frac{x^2}{(x+y)^2} - \delta x \\ -\frac{y^2}{(x+y)^2} - y & 1 - \frac{x^2}{(x+y)^2} - (x+2y) \end{pmatrix}. \quad (12)$$

At E_1 , the matrix is

$$\mathcal{J}(E_1) = \begin{pmatrix} -\beta & -2\beta \\ 0 & -\beta/\delta \end{pmatrix},$$

with eigenvalues $-\beta < 0$ and $-\beta/\delta < 0$, implying that E_1 is a sink. At E_2 , the matrix takes the form

$$\mathcal{J}(E_2) = \begin{pmatrix} -\delta & 0 \\ -2 & -1 \end{pmatrix}.$$

Hence, again, E_2 is a sink.

By (12), the Jacobian matrix at E^* is

$$\mathcal{J}(E^*) = \frac{\beta}{(\beta + \delta)^2} \begin{pmatrix} \delta(\beta - \delta) & -2\delta^2 \\ -2\beta & \delta - \beta \end{pmatrix} := \frac{\beta}{(\beta + \delta)^2} \tilde{\mathcal{J}}(E^*). \quad (13)$$

It is easy to calculate the characteristic polynomial of $\tilde{\mathcal{J}}(E^*)$ in (13) as

$$\phi(\lambda) = \lambda^2 + (1 - \delta)(\beta - \delta)\lambda - \delta(\beta + \delta)^2,$$

which has positive discriminant, and hence the roots of $\phi(\lambda) = 0$ are real. Since $\det \mathcal{J}(E^*) = -\beta^2\delta/(\beta + \delta)^2 < 0$, we have that E^* is a saddle. This completes the proof. \square

The stable curve of E^* , denoted by $y = h(x)$, plays a key role in characterizing the global dynamics of System (10): solutions initiated above $y = h(x)$ tend to E_2 , and otherwise to E_1 . The basins of attraction of E_1 and E_2 , denoted by $\mathcal{B}(E_1)$ and $\mathcal{B}(E_2)$, are then defined by

$$\mathcal{B}(E_1) = \{(x, y) : x > 0, 0 \leq y < h(x)\}, \mathcal{B}(E_2) = \{(x, y) : x \geq 0, y > h(x)\}. \tag{14}$$

The x -isocline $x = \delta/\beta(x + y)^2$ and the y -isocline $y = (x + y)^2$ intersect at $E_0 = (0, 0)$ and $E^* = (x^*, y^*)$, which decompose the first quadrant into four basic regions:

$$\begin{aligned} D_1 &= \{(x, y) : f(x, y) > 0, g(x, y) > 0\}, \\ D_2 &= \{(x, y) : 0 \leq y < y^*, g(x, y) \leq x \leq f(x, y)\}, \\ D_3 &= \{(x, y) : f(x, y) < 0, g(x, y) < 0\}, \\ D_4 &= \{(x, y) : 0 \leq x < x^*, f(x, y) \leq y \leq g(x, y)\}. \end{aligned}$$

To locate $h(x)$, we check the direction field of System (10), and find that $D_2 \subset \mathcal{B}(E_1)$ and $D_4 \subset \mathcal{B}(E_2)$. Hence $h(x)$ must lie in D_1 and D_3 separately. See Figure 2 below.

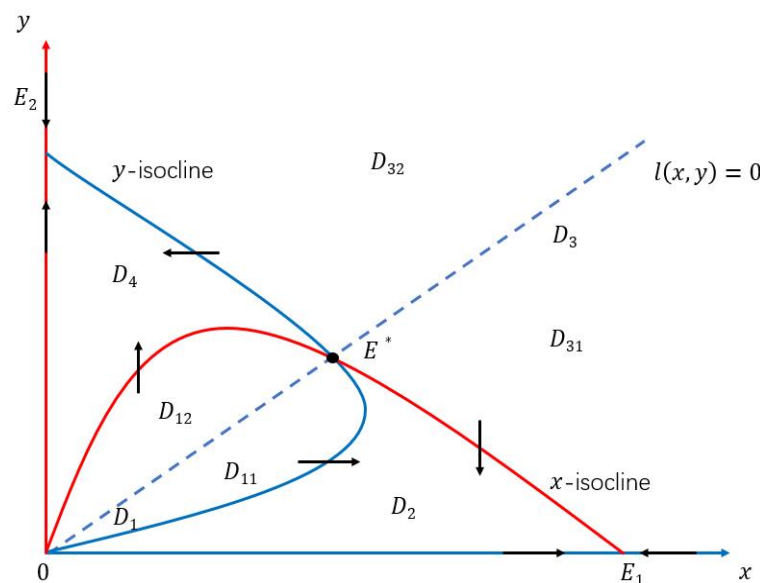


Figure 2. State domain decomposition by the x -isocline $x = \delta/\beta(x + y)^2$, the y -isocline $y = (x + y)^2$, and the straight line $\beta x - \delta y = 0$. The stable curve W^s coincides with \mathcal{L} when $\delta = 1$ lies entirely in D_{12} and D_{31} when $\delta > 1$, and lies entirely in D_{11} and D_{32} when $\delta < 1$.

It is easy to see that solutions lying in D_1 or D_3 satisfy

$$\frac{dy}{dx} = \frac{g(x, y)}{f(x, y)} > 0.$$

Hence, the stable curve can be expressed as a smooth and strictly increasing function $y = h(x)$. In D_1 , note that if $(x(t), y(t))$ tends toward E_0 in backward time, then the α -limit set of the stable curve must be E_0 . Thus, the curve is also the heteroclinic orbit connecting E_0 and E^* . In D_3 , both x' and y' are negative, so we are still concerned with α -limit set of $(x(t), y(t))$. Denote

$$\lim_{t \rightarrow -\infty} (x(t), y(t)) = (x_\infty, y_\infty).$$

In addition, we claim that both x_∞ and y_∞ are infinity. Otherwise, since there is no equilibrium in D_3 , either x_∞ or y_∞ must be infinity. If $x_\infty < y_\infty = \infty$, then by substituting x_∞ and y_∞ into (10) we get $dx/dt = \infty$ as $t \rightarrow -\infty$. On the other hand, because $x_\infty < \infty$, we

can infer $dx/dt = 0$ as $t \rightarrow -\infty$, which yields a contradiction. Continuing in this fashion, we can also derive $y_\infty = \infty$.

In summary, in the first quadrant $R_+^2 = \{(x, y) : x \geq 0, y \geq 0\}$, the stable curve of E^* is given by

$$W^s(E^*) = \{(x, y) : y = h(x), h(0) = 0, h(x^*) = y^*\},$$

where the function h is smooth. Furthermore, it satisfies

$$h'(x) > 0 \text{ for } x > 0, \text{ and } \lim_{x \rightarrow \infty} h(x) = \infty,$$

such that the portion of $W^s(E^*)$ for $0 < x < x^*$ defines the heteroclinic orbit connecting the trivial equilibrium E_0 and E^* , and the portion of $W^s(E^*)$ for $x > x^*$ defines the other branch of the stable curve. Since it is usually a formidable task to compute the exact form of $h(x)$, we get around this difficulty by finding sharp estimates of $y = h(x)$ in the following theorem.

Theorem 2. Define

$$h_0(x) = \frac{\beta x}{\delta} \text{ and } h_1(x) = \frac{\beta^2}{(\beta + \delta)^2} \left(\frac{(\beta + \delta)^2 x}{\beta \delta} \right)^{1/\delta},$$

and then $h = h_0 = h_1$ at $x = 0$ and $x = x^*$, and $h(x)$ is sandwiched between h_0 and h_1 . When $\delta = 1$, the three functions are identical, and the curve $W^s(E^*)$ coincides with the straight line

$$\mathcal{L} : l(x, y) := \beta x - \delta y = 0. \tag{15}$$

When $\delta > 1$, we have

$$h_0(x) < h(x) < h_1(x) \text{ for } 0 < x < x^*, \text{ and } h_1(x) < h(x) < h_0(x) \text{ for } x > x^*. \tag{16}$$

When $\delta < 1$, we have

$$h_1(x) < h(x) < h_0(x) \text{ for } 0 < x < x^*, \text{ and } h_0(x) < h(x) < h_1(x) \text{ for } x > x^*. \tag{17}$$

Proof. To locate $y = h(x)$, we divide D_1 into

$$D_{11} = \left\{ (x, y) : (x, y) \in D_1, 0 < y < \frac{\beta}{\delta} x \right\},$$

and

$$D_{12} = \left\{ (x, y) : (x, y) \in D_1, y > \frac{\beta}{\delta} x \right\}.$$

Similarly, we denote the subregion of D_3 below \mathcal{L} as D_{31} , and the subregion above \mathcal{L} as D_{32} (see Figure 2).

When $\delta = 1$, we claim that the straight line \mathcal{L} coincides with $W^s(E^*)$. In fact, on the straight line \mathcal{L} , we have $\beta x = \delta y$ and $x + y = (1 + \beta/\delta)x$. For $l(x, y)$ defined in (15), we have

$$\begin{aligned} \left. \frac{dl}{dt} \right|_{\mathcal{L}} &= \beta x \left(\beta - \frac{\beta y}{x + y} - \delta(x + y) \right) - \delta y \left(1 - \frac{x}{x + y} - (x + y) \right) \\ &= \beta x \left((\beta - 1) + \frac{1}{x + y} (x - \beta y) + (1 - \delta)(x + y) \right) \\ &= \beta x \left(\frac{\beta(\delta - 1)}{\beta + \delta} + (1 - \delta) \frac{\beta + \delta}{\beta} y \right) \\ &= (1 - \delta)(\beta + \delta)(y - y^*)x = 0, \end{aligned} \tag{18}$$

showing that \mathcal{L} consists of solutions of (10). Hence the curve $W^s(E^*)$ coincides with the line \mathcal{L} , and the three functions h_0, h , and h_1 are identical. Moreover, we expect that the direction vector of \mathcal{L} must be an eigenvector of $\mathcal{J}(E^*)$ defined in (13). Indeed, by direct calculation we find

$$\begin{aligned} \mathcal{J}(E^*) \begin{pmatrix} \delta \\ \beta \end{pmatrix} &= \frac{1}{(\beta + \delta)^2} \begin{pmatrix} \beta\delta(\beta + \delta)^2 - \beta^3\delta - \beta\delta^2(\beta + 2\delta) - 2\beta^2\delta^2 \\ -2\beta^2\delta + \beta(\beta + \delta)^2 - \beta\delta^2 - \beta^2(2\beta + \delta) \end{pmatrix} \\ &= \frac{1}{(\beta + \delta)^2} \begin{pmatrix} -\beta\delta^3 - \beta^2\delta^2 \\ -\beta^3 - \delta\beta^2 \end{pmatrix} \\ &= -\frac{\beta}{(\beta + \delta)} \begin{pmatrix} \delta \cdot \delta \\ \beta \end{pmatrix}. \end{aligned} \tag{19}$$

It follows from (19) that the direction vector of \mathcal{L} is an eigenvector of $\mathcal{J}(E^*)$ if and only if $\delta = 1$.

For the case with $\delta \neq 1$, equality (18) implies that $W^s(E^*)$ does not coincide with the straight line \mathcal{L} anymore. For an arbitrary solution $(x(t), y(t))$ of (10) with $f \neq 0$, we have $dy/dx = g/f$. To locate $y = h(x)$, we compute the d^2y/dx^2 from

$$\frac{df}{dx} = \frac{f}{x} - \frac{\beta x^2 g f^{-1} - \beta x y}{(x + y)^2} - \delta x(1 + g f^{-1}) \text{ and } \frac{dg}{dx} = \frac{g^2}{y f} - \frac{y^2 - x y g f^{-1}}{(x + y)^2} - y(1 + g f^{-1}).$$

Therefore,

$$\begin{aligned} \frac{d^2y}{dx^2} &= \frac{1}{f} \frac{dg}{dx} - \frac{g}{f^2} \frac{df}{dx} \\ &= \frac{1}{f} \left(\frac{g^2}{y f} - \frac{y^2 - x y g f^{-1}}{(x + y)^2} - y(1 + g f^{-1}) \right) - \frac{g}{f^2} \left(\frac{f}{x} - \frac{\beta x^2 g f^{-1} - \beta x y}{(x + y)^2} - \delta x(1 + g f^{-1}) \right) \\ &= \left(\frac{g}{f^2} + \frac{x y (y + \beta x g f^{-1})}{(x + y)^2 f^2} \right) \left(\frac{g}{y} - \frac{f}{x} \right) - \frac{\delta x y}{f^2} (1 + g f^{-1}) \left(\frac{f}{\delta x} - \frac{g}{y} \right). \end{aligned}$$

Recalling $l(x, y)$ defined in (15), we find

$$\frac{f}{\delta x} - \frac{g}{y} = \frac{l(x, y)}{\delta(x + y)}, \tag{20}$$

and hence

$$\frac{d^2y}{dx^2} = \left(\frac{g}{f^2} + \frac{x y (y + \beta x g f^{-1})}{(x + y)^2 f^2} \right) \left(\frac{g}{y} - \frac{f}{x} \right) - \frac{\delta x y}{f^2} (1 + g f^{-1}) \left(\frac{l(x, y)}{\delta(x + y)} \right). \tag{21}$$

When $\delta > 1$, since $l(x, y) > 0$ and $f > 0$ in D_{11} , it follows from (20) that

$$\frac{g}{y} - \frac{f}{x} < \frac{g}{y} - \frac{1}{\delta} \frac{f}{x} = -\frac{l(x, y)}{\delta(x + y)} < 0. \tag{22}$$

Combined with (22), (21) gives $d^2y/dx^2 < 0$, which implies that the solution is concave-down in D_{11} . Now we assume that if the stable curve has a segment lying in D_{11} , then there are $x_1, x_2 \in (0, x^*)$ with $x_1 < x_2$, such that both $(x_1, h(x_1))$ and $(x_2, h(x_2))$ stay on \mathcal{L} , and $y = h(x)$ stays below \mathcal{L} for $x \in (x_1, x_2)$. This contradicts the fact that $y = h(x)$ is concave-down in D_{11} . Then, we can conclude that the heteroclinic orbit connecting E_0 and E^* must lie entirely in D_{12} .

To find an upper bound of $h(x)$ in D_{12} , we introduce

$$z(t) = \ln [x(t)^{1/\delta} y(t)^{-1}]. \tag{23}$$

By visiting (10), we find

$$z'(t) = \frac{x'}{\delta x} - \frac{y'}{y} = \frac{\beta x - \delta y}{\delta(x+y)} = \frac{l(x,y)}{\delta(x+y)}. \tag{24}$$

Since $l(x,y) < 0$ for all $(x,y) \in D_{12}$, we see that

$$z'(t) = \frac{l(x,y)}{\delta(x+y)} < 0.$$

Thus $z(t)$ decreases monotonically with t in D_{12} , leading to $z(t) > \lim_{t \rightarrow \infty} z(t)$, and therefore

$$x^{1/\delta} h(x)^{-1} > (x^*)^{1/\delta} (y^*)^{-1} \text{ or } h(x) < y^* (x/x^*)^{1/\delta}, \quad 0 < x < x^*.$$

By substituting x^* and y^* into the last inequality, we get

$$h(x) < h_1 = \frac{\beta^2}{(\beta + \delta)^2} \left(\frac{(\beta + \delta)^2 x}{\beta \delta} \right)^{1/\delta}, \quad 0 < x < x^*. \tag{25}$$

Heretofore we have verified the first part of (16).

For the second part of (16), we use the properties of the eigenvectors of $\mathcal{J}(E^*)$ to analyze the behavior of $h(x)$ in D_3 . It follows from (19) that the direction vector of \mathcal{L} is not an eigenvector of $\mathcal{J}(E^*)$ for $\delta > 1$, which implies that \mathcal{L} is not tangential to the stable curve $h(x)$ at E^* . Hence the stable curve lies in D_{31} when $x > x^*$ with x being sufficiently close to x^* . Actually, the stable curve will always stay in D_{31} for all $x > x^*$. To see this, we recall (18) and find that all trajectories initiated at \mathcal{L} with $y > y^*$ move into D_{32} when t increases from $t = 0$. Hence, the stable curve cannot meet \mathcal{L} from the domain D_{31} when x increases, or equivalently, when t decreases. As $l(x,y) > 0$ in D_{31} , $z(t)$ increases strictly along the stable curve in this domain, giving $z(t) < \lim_{t \rightarrow \infty} z(t)$. By the same calculation of deriving (25), we obtain the estimate

$$h(x) > h_1(x), \quad x > x^*,$$

and complete the proof of (16).

Next, we consider the case $\delta < 1$. Since $l(x,y) < 0$ and $f > 0$ in D_{12} , it follows from (20) that

$$\frac{g}{y} - \frac{f}{x} > \frac{g}{y} - \frac{1}{\delta} \frac{f}{x} = -\frac{l(x,y)}{\delta(x+y)} > 0.$$

Now (21) gives $d^2y/dx^2 > 0$, resulting in the solution that is concave-up in D_{12} . If the stable curve has a segment lying in D_{12} , then there are $x_1, x_2 \in (0, x^*)$ with $x_1 < x_2$, such that both $(x_1, h(x_1))$ and $(x_2, h(x_2))$ stay on \mathcal{L} , and $y = h(x)$ stays above \mathcal{L} for $x \in (x_1, x_2)$. This yields a contradiction because the secant line \mathcal{L} cannot be located below the concave-up curve $y = h(x)$ over (x_1, x_2) . Therefore, we find that the heteroclinic orbit connecting E_0 and E^* must lie entirely in D_{11} in this case.

Since $l(x,y) > 0$ for all $(x,y) \in D_{11}$, it follows from (24) that $z(t)$ increases along the heteroclinic orbit. Hence $z(t) < \lim_{t \rightarrow \infty} z(t)$, and with the same process yielding (25) we derive

$$h(x) > h_1(x), \quad 0 < x < x^*. \tag{26}$$

Again, the direction vector of \mathcal{L} is not an eigenvector of $\mathcal{J}(E^*)$ for $\delta < 1$; thus, the stable curve lies in D_{32} when $x > x^*$ with x being sufficiently close to x^* . Therefore, (18) gives that all trajectories initiated at \mathcal{L} with $y > y^*$ must move into D_{31} when t increases from $t = 0$, which implies that the stable curve cannot meet \mathcal{L} from the domain D_{32} as t decreases. This ensures that the stable curve stays in D_{32} for all $x > x^*$. As $l(x,y) < 0$ in

D_{32} , $z(t)$ decreases strictly along the stable curve in this domain, giving $z(t) > \lim_{t \rightarrow \infty} z(t)$, and

$$h(x) < h_1(x), \quad x > x^*. \tag{27}$$

Combining (26) and (27), we have (17), proving the theorem. \square

Mathematically, by finding two exclusive regions $\mathcal{B}(E_1)$ and $\mathcal{B}(E_2)$ in (14), Theorems 1 and 2 offer a complete characterization of the global dynamics between two *Wolbachia* strains with complete CI. Biologically, these two theorems indicate that once the parameter values and the initial population sizes lie in $\mathcal{B}(E_1)$, then *w-A* strain outcompetes the *w-B* strain eventually. Otherwise, the *w-B* strain washes out the *w-A* strain.

3.2. System (9) with Incomplete CI

Complete CI makes eggs produced from incompatible matings that do not hatch. However, incomplete CI is much more common in *Wolbachia* hosts. For example, the authors in [11] scored 2972 eggs from the incompatible matings for the *wRi* in *Aedes albopictus*; 422 of them survived from CI and hatched. The *Wolbachia* strain *cifB* in *Anopheles gambiae* [46], and *wPip* in *Culex pipiens* [47] also fail to induce complete CI. To explore the effect of incomplete CI on the global dynamics of *Wolbachia*, in this subsection, we study System (9) with $s_h^A, s_h^B \in (0, 1)$. It is trivial that $E_0 = (0, 0)$ is an equilibrium of System (9). Any other equilibria of System (9) satisfy

$$x \left(\beta - \beta s_h^A \frac{y}{x+y} - \delta(x+y) \right) = 0, \tag{28}$$

and

$$y \left(1 - s_h^B \frac{x}{x+y} - (x+y) \right) = 0, \tag{29}$$

which admits two boundary equilibria $\tilde{E}_1 = (\beta/\delta, 0)$ and $\tilde{E}_2 = (0, 1)$. It follows from (28) and (29) that any interior equilibrium point satisfies

$$(\beta - \delta) + \delta s_h^B \frac{x}{x+y} - \beta s_h^A \frac{y}{x+y} = 0,$$

which leads to

$$y = \frac{\beta + \delta s_h^B - \delta}{\delta + \beta s_h^A - \beta} x. \tag{30}$$

Substituting (30) into (29), we get

$$\tilde{E}^* = \left(\frac{\beta(\delta + \beta s_h^A - \beta)(s_h^A + s_h^B - s_h^A s_h^B)}{(\beta s_h^A + \delta s_h^B)^2}, \frac{\beta(\beta + \delta s_h^B - \delta)(s_h^A + s_h^B - s_h^A s_h^B)}{(\beta s_h^A + \delta s_h^B)^2} \right).$$

To unload the notation burden, we let $\kappa_1 = \delta + \beta s_h^A - \beta$, $\kappa_2 = \beta + \delta s_h^B - \delta$, and $c = s_h^A + s_h^B - s_h^A s_h^B$. Then, the interior equilibrium reads as

$$\tilde{E}^* = \left(\frac{\beta \kappa_1 c}{(\kappa_1 + \kappa_2)^2}, \frac{\beta \kappa_2 c}{(\kappa_1 + \kappa_2)^2} \right). \tag{31}$$

When $\beta = \delta$, we have $\kappa_1 = \beta s_h^A > 0$ and $\kappa_2 = \delta s_h^B > 0$. If $\beta > \delta$, we define

$$s_A^* = \frac{\beta - \delta}{\beta},$$

and if $\delta > \beta$, we define

$$s_B^* = \frac{\delta - \beta}{\delta}.$$

Then \tilde{E}^* lies in the first quadrant when either

$$\beta > \delta \text{ and } s_h^A > s_A^*,$$

or

$$\beta < \delta \text{ and } s_h^B > s_B^*$$

holds.

To analyze the stability of the equilibria, we calculate the Jacobian matrix of (9) as

$$\tilde{\mathcal{J}}(x, y) = \begin{pmatrix} \beta \left(1 - \frac{s_h^A y^2}{(x+y)^2} \right) - \delta(2x+y) & -\beta s_h^A \frac{x^2}{(x+y)^2} - \delta x \\ -s_h^B \frac{y^2}{(x+y)^2} - y & 1 - s_h^B \frac{x^2}{(x+y)^2} - (x+2y) \end{pmatrix}. \tag{32}$$

Next, we count the number of equilibria of System (9) and analyze the corresponding stability in three different cases in terms of the comparison between the magnitude of β and δ , namely, $\beta = \delta$, $\beta > \delta$ and $\beta < \delta$.

Case I. $\beta = \delta$. In this case, System (9) has four equilibria on the first quadrant, $\tilde{E}_0 = (0, 0)$, $\tilde{E}_1 = (\beta/\delta, 0)$, $\tilde{E}_2 = (0, 1)$, and

$$\tilde{E}^* = (\tilde{x}^*, \tilde{y}^*) = \left(\frac{s_h^A c}{(s_h^A + s_h^B)^2}, \frac{s_h^B c}{(s_h^A + s_h^B)^2} \right).$$

Similar to the proof of Theorem 1, we can prove that \tilde{E}_0 is unstable. Substituting \tilde{E}_1 into (32), we have

$$\tilde{\mathcal{J}}(\tilde{E}_1) = \begin{pmatrix} -\beta & -(s_h^A + 1)\beta \\ 0 & -\kappa_2/\delta \end{pmatrix}, \tag{33}$$

with eigenvalues $-\beta < 0$ and $-\kappa_2/\delta = -s_h^B < 0$, implying that \tilde{E}_1 is a sink. At \tilde{E}_2 , the Jacobian matrix takes the form

$$\tilde{\mathcal{J}}(\tilde{E}_2) = \begin{pmatrix} -\kappa_1 & 0 \\ -s_h^B - 1 & -1 \end{pmatrix}. \tag{34}$$

Since $-\kappa_1 = -\beta s_h^A < 0$, \tilde{E}_2 is also a sink. The Jacobian matrix at \tilde{E}^* takes the form

$$\tilde{\mathcal{J}}(\tilde{E}^*)|_{\beta=\delta} = \frac{\beta}{(s_h^A + s_h^B)^2} \begin{pmatrix} (s_h^A + s_h^B)^2 - s_h^A (s_h^B)^2 - (2s_h^A + s_h^B)c & -\beta (s_h^A)^3 - s_h^A c \\ -(s_h^B)^3 - s_h^B c & (s_h^A + s_h^B)^2 - (s_h^A)^2 s_h^B - (s_h^A + 2s_h^B)c \end{pmatrix}.$$

Direct calculation yields $\det \tilde{\mathcal{J}}(\tilde{E}^*)|_{\beta=\delta} = -c\beta^5 s_h^A s_h^B (s_h^A + s_h^B)^2 < 0$, and hence, \tilde{E}^* is a saddle.

Case II. $\beta > \delta$. In such a situation, we have three subcases. The first one is when $s_h^A > s_A^*$, and System (9) has \tilde{E}^* defined in (31) lying in the first quadrant. The origin \tilde{E}_0 is a source. It follows from (33) and (34) that both \tilde{E}_1 and \tilde{E}_2 are sinks since $\kappa_1 > 0$ and $\kappa_2 > 0$. At \tilde{E}^* with $\beta > \delta$, we have

$$\tilde{\mathcal{J}}(\tilde{E}^*)|_{\beta>\delta} = \begin{pmatrix} \beta(\kappa_1 + \kappa_2)^2 - \beta s_h^A \kappa_2^2 - \delta \beta c(2\kappa_1 + \kappa_2) & -\beta s_h^A \kappa_1^2 + \delta \beta \kappa_1 c \\ -s_h^B \kappa_2^2 - \beta \kappa_2 c & (\kappa_1 + \kappa_2)^2 - s_h^B \kappa_1^2 - \beta c(2\kappa_2 + \kappa_1) \end{pmatrix}.$$

Tedious but simple calculation reaches $\delta \tilde{\mathcal{J}}(\tilde{E}^*)|_{\beta > \delta} = -\beta c(\kappa_1 + \kappa_2)^2 \kappa_1 \kappa_2 < 0$, and hence \tilde{E}^* is a saddle if $s_h^A > s_A^*$.

If $s_h^A = s_A^*$, then $\kappa_1 = 0$ and $\tilde{E}^* = \tilde{E}_2 = (0, 1)$. By analyzing the direction field (see Figure 3A) of System (9), we find that for any small $\varepsilon > 0$, any solution of System (9) initiated from $U_\varepsilon = \{(x, y) | x^2 + (y - 1)^2 < \varepsilon\}$ will eventually exit from U_ε , implying the instability of \tilde{E}_2 .

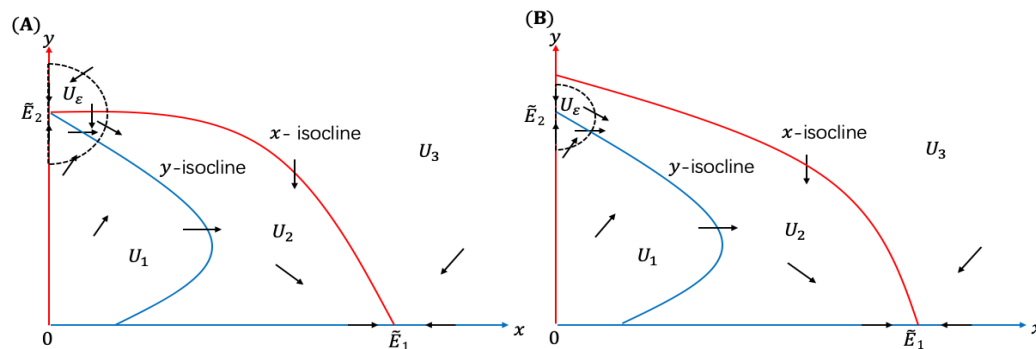


Figure 3. The direction field of System (9) with $\beta > \delta$. Panel (A) is for $s_h^A = s_A^*$, and panel (B) is for $s_h^A < s_A^*$.

To investigate the stability of \tilde{E}_1 , we denote

$$\begin{aligned}
 U_1 &= \{(x, y) : F(x, y) > 0, G(x, y) > 0\}, \\
 U_2 &= \{(x, y) : F(x, y) > 0, G(x, y) < 0\}, \\
 U_3 &= \{(x, y) : F(x, y) < 0, G(x, y) < 0\}.
 \end{aligned}$$

By graphing the direction field in these subregions, we find that U_2 is the basin of attraction of \tilde{E}_1 . Furthermore, solutions of System (9) initiated from U_1 or U_3 will enter U_2 in the finite time, and then tends to \tilde{E}_1 as $t \rightarrow +\infty$. These observations prove that \tilde{E}_1 is a sink, which is globally asymptotically stable.

If $s_h^A < s_A^*$, then $\kappa_1 < 0$, and \tilde{E}^* stays in the second quadrant. In this case, following the same procedure as Case II, with the help of the direction field plotted in Figure 3B, we can prove that \tilde{E}_1 is globally asymptotically stable, and \tilde{E}_2 is a saddle. It is obvious that when $s_h^A \leq s_A^*$, \tilde{E}_0 is a source.

Case III. Following the lines in Case II, we can count the number of equilibria and analyze their corresponding stability, and we omit it here. To make the conclusions concise, we summarize the above analysis in Table 3.

Table 3. Condition for the existence and stability of equilibria of System (9).

| Condition on β, δ | Condition on s_h^A, s_h^B | Equilibria and Stability |
|------------------------------|-----------------------------|---|
| $\beta = \delta$ | $0 < s_h^A, s_h^B < 1$ | \tilde{E}_0 source, \tilde{E}_1 sink, \tilde{E}_2 sink, \tilde{E}^* saddle |
| $\beta > \delta$ | $s_h^A < s_A^*$ | \tilde{E}_0 source, \tilde{E}_1 globally asymptotically stable sink, \tilde{E}_2 saddle |
| | $s_h^A = s_A^*$ | \tilde{E}_0 source, \tilde{E}_1 globally asymptotically stable sink, \tilde{E}_2 unstable |
| | $s_h^A > s_A^*$ | \tilde{E}_0 source, \tilde{E}_1 sink, \tilde{E}_2 sink, \tilde{E}^* saddle |
| $\beta < \delta$ | $s_h^B < s_B^*$ | \tilde{E}_0 source, \tilde{E}_1 saddle, \tilde{E}_2 globally asymptotically stable sink |
| | $s_h^B = s_B^*$ | \tilde{E}_0 source, \tilde{E}_1 unstable, \tilde{E}_2 globally asymptotically stable sink |
| | $s_h^B > s_B^*$ | \tilde{E}_0 source, \tilde{E}_1 sink, \tilde{E}_2 sink, \tilde{E}^* saddle |

Biologically, what we are concerned about most is the outcome of the competition between two *Wolbachia* strains, that is, which strain will outcompete the other one. Mathematically, the fate of each strain is completely determined by whether or not the initial population size lies in the basin of attraction of \tilde{E}_1 or \tilde{E}_2 , denoted by $\mathcal{B}(\tilde{E}_1)$ or $\mathcal{B}(\tilde{E}_2)$, respectively. The introduction of the incomplete CI makes the characterization of $\mathcal{B}(\tilde{E}_1)$ and $\mathcal{B}(\tilde{E}_2)$ much more complex than the case of complete CI. However, the summary in Table 3 leads to the following results.

Theorem 3. (1) If $\beta > \delta$, $s_h^A \leq s_A^*$, then $\mathcal{B}(\tilde{E}_1) = \{(x, y) : x > 0, y \geq 0\}$, and $\mathcal{B}(\tilde{E}_2) = \{(x, y) : x = 0, y > 0\}$.

(2) If $\beta < \delta$, $s_h^B \leq s_B^*$, then $\mathcal{B}(\tilde{E}_1) = \{(x, y) : x > 0, y = 0\}$, and $\mathcal{B}(\tilde{E}_2) = \{(x, y) : x \geq 0, y > 0\}$.

To make the characterization of $\mathcal{B}(\tilde{E}_1)$ and $\mathcal{B}(\tilde{E}_2)$ complete, we still have three cases to consider:

$$(i) \beta = \delta, (ii) \beta > \delta \text{ and } s_h^A > s_A^*, \text{ and } (iii) \beta < \delta \text{ and } s_h^B > s_B^*. \tag{35}$$

For these three cases, the outcome of the competition between two *Wolbachia*-strains is uncertain, which depends on the position of the initial population size (x_0, y_0) . If $(x_0, y_0) \in \mathcal{B}(\tilde{E}_1)$, then *w*-A wins. If $(x_0, y_0) \in \mathcal{B}(\tilde{E}_2)$, then *w*-B wins, as shown in Theorem 3. The separatrix of $\mathcal{B}(\tilde{E}_1)$ and $\mathcal{B}(\tilde{E}_2)$ is exactly the stable curve of the saddle \tilde{E}^* , denoted by \tilde{h} . Next, we offer a relatively sharp estimation of \tilde{h} . Based on the location of \tilde{h} , we have

$$\mathcal{B}(\tilde{E}_1) = \{(x, y) : x > 0, 0 \leq y < \tilde{h}(x)\}, \mathcal{B}(\tilde{E}_2) = \{(x, y) : x \geq 0, y > \tilde{h}(x)\}.$$

For cases in (35), the *x*-isocline $\beta x + \beta(1 - s_h^A)y = \delta(x + y)^2$ and the *y*-isocline $(1 - s_h^B)x + y = (x + y)^2$ intersect at $\tilde{E}_0 = (0, 0)$ and $\tilde{E}^* = (\tilde{x}^*, \tilde{y}^*)$, which decompose the first quadrant into four basic regions:

$$\begin{aligned} \tilde{D}_1 &= \{(x, y) : F(x, y) > 0, G(x, y) > 0\}, \\ \tilde{D}_2 &= \{(x, y) : F(x, y) > 0, G(x, y) < 0\}, \\ \tilde{D}_3 &= \{(x, y) : F(x, y) < 0, G(x, y) < 0\}, \\ \tilde{D}_4 &= \{(x, y) : F(x, y) < 0, G(x, y) > 0\}. \end{aligned}$$

To locate $\tilde{h}(x)$, we check the direction field of System (10), and find that $\tilde{D}_2 \subset \mathcal{B}(\tilde{E}_1)$ and $\tilde{D}_4 \subset \mathcal{B}(\tilde{E}_2)$. Hence, $\tilde{h}(x)$ must lie in \tilde{D}_1 and \tilde{D}_3 separately. See Figure 4 below.

Similar to the proof of Theorem 2, we have the following.

Theorem 4. Define

$$\tilde{h}_0(x) = \frac{\kappa_2}{\kappa_1}x \text{ and } \tilde{h}_1(x) = \frac{\beta\kappa_2c}{(\kappa_1 + \kappa_2)^2} \left(\frac{(\kappa_1 + \kappa_2)^2x}{\beta\kappa_1c} \right)^{1/\delta},$$

and then $\tilde{h} = \tilde{h}_0 = \tilde{h}_1$ at $x = 0$ and $x = \tilde{x}^*$, and $\tilde{h}(x)$ is sandwiched between \tilde{h}_0 and \tilde{h}_1 . When $\delta = 1$, the three functions are identical, and the curve $\tilde{h}(x)$ coincides with the straight line

$$\tilde{\mathcal{L}} : \tilde{l}(x, y) := \kappa_2x - \kappa_1y = 0. \tag{36}$$

When $\delta > 1$, we have

$$\tilde{h}_0(x) < \tilde{h}(x) < \tilde{h}_1(x) \text{ for } 0 < x < \tilde{x}^*, \text{ and } \tilde{h}_1(x) < \tilde{h}(x) < \tilde{h}_0(x) \text{ for } x > \tilde{x}^*. \tag{37}$$

When $\delta < 1$, we have

$$\tilde{h}_1(x) < \tilde{h}(x) < \tilde{h}_0(x) \text{ for } 0 < x < \tilde{x}^*, \text{ and } \tilde{h}_0(x) < h(x) < \tilde{h}_1(x) \text{ for } x > \tilde{x}^*. \quad (38)$$

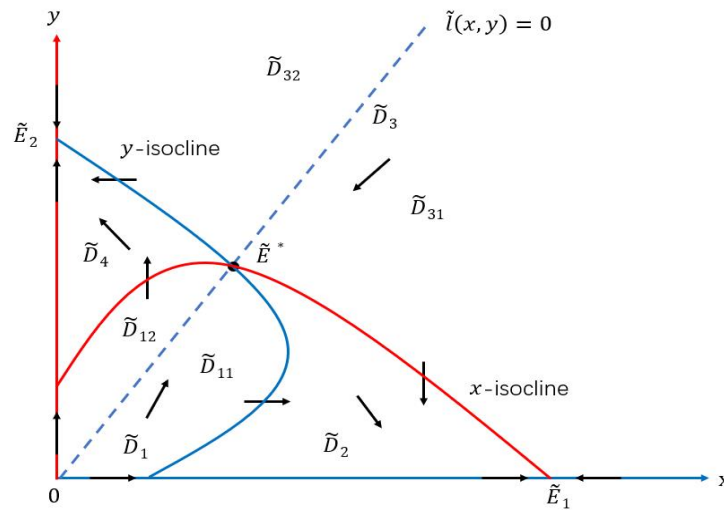


Figure 4. State domain decomposition by the x -isocline $\beta x + \beta(1 - s_h^A)y = \delta(x + y)^2$, the y -isocline $(1 - s_h^B)x + y = (x + y)^2$, and the straight line $\kappa_2 x - \kappa_1 y = 0$. The stable curve W^s coincides with \mathcal{L} when $\delta = 1$, lies entirely in \tilde{D}_{12} and \tilde{D}_{31} when $\delta > 1$, and lies entirely in \tilde{D}_{11} and \tilde{D}_{32} when $\delta < 1$.

Proof. The region \tilde{D}_1 can be further divided into

$$\tilde{D}_{11} = \left\{ (x, y) : (x, y) \in \tilde{D}_1, 0 < y < \frac{\kappa_2}{\kappa_1} x \right\},$$

and

$$\tilde{D}_{12} = \left\{ (x, y) : (x, y) \in \tilde{D}_1, y > \frac{\kappa_2}{\kappa_1} x \right\}.$$

Similarly, the region \tilde{D}_3 is divided into \tilde{D}_{31} and \tilde{D}_{32} by $\tilde{\mathcal{L}}$ (see Figure 4). When $\delta = 1$, we have

$$\begin{aligned} \left. \frac{dl}{dt} \right|_{\mathcal{L}} &= \kappa_2 x \left(\beta - \frac{\beta s_h^A y}{x + y} - \delta(x + y) \right) - \kappa_1 y \left(1 - \frac{s_h^B x}{x + y} - (x + y) \right) \\ &= \kappa_2 x \left((\beta - 1) + \frac{s_h^B x - \beta s_h^A y}{x + y} + (1 - \delta)(x + y) \right) \\ &= (1 - \delta)(\kappa_1 + \kappa_2)x \left(y - \frac{\beta \kappa_1}{(\kappa_1 + \kappa_2)^2} \right) \\ &= (1 - \delta)(\kappa_1 + \kappa_2)x(y - y^*) = 0, \end{aligned} \quad (39)$$

showing that $\tilde{\mathcal{L}}$ is a special solution of (9). Hence, $\tilde{h}(x)$ coincides with the line $\tilde{\mathcal{L}}$. Meanwhile, the direct calculation yields

$$\begin{aligned} J(E^*) \begin{pmatrix} \kappa_1 \\ \kappa_2 \end{pmatrix} &= \frac{1}{(\kappa_1 + \kappa_2)^2} \begin{pmatrix} \beta \left(\kappa_2 \left((\kappa_1 + \kappa_2)^2 - s_h^A \kappa_2^2 - \delta c(2\kappa_1 + \kappa_1) \right) - \kappa_2 (s_h^A \kappa_1 + \delta \kappa_1 c) \right) \\ \kappa_1 \left(-s_h^B \kappa_2^2 - \beta \kappa_2 s \right) + \kappa_2 \left((\kappa_1 + \kappa_2)^2 - s_h^B \kappa_1^2 - \beta c(\kappa_1 + 2\kappa_2) \right) \end{pmatrix} \\ &= \frac{1}{\kappa_1 + \kappa_2} \begin{pmatrix} \beta \kappa_1 (\kappa_1 + \kappa_2 - s_1 \kappa_2 - 2\delta c) \\ \kappa_2 (-2\beta c + \kappa_1 + \kappa_2 - s_h^B \kappa_1) \end{pmatrix} = \frac{-\beta c}{\kappa_1 + \kappa_2} \begin{pmatrix} \delta \kappa_1 \\ \kappa_2 \end{pmatrix}, \end{aligned}$$

proving that $\tilde{\mathcal{L}}$ is an eigenvector of $\mathcal{J}(\tilde{E}^*)$ if and only if $\delta = 1$.

If $\delta \neq 1$, then with (36) we get

$$\begin{aligned}
 \frac{d^2y}{dx^2} &= \frac{1}{F} \frac{dG}{dx} - \frac{G}{F^2} \frac{dF}{dx} \\
 &= \frac{1}{F} \left(\frac{G^2}{yF} - s_h^B y \frac{y - GF^{-1}x}{(x+y)^2} - y(1 + GF^{-1}) \right) - \frac{G}{F^2} \left(\frac{F}{x} + \beta s_h^A x \frac{y - xGF^{-1}}{(x+y)^2} - \delta x(1 + GF^{-1}) \right) \\
 &= \left(\frac{G}{F^2} + \frac{xy(s_h^B y + \beta s_h^A GF^{-1}x)}{(x+y)^2 F^2} \right) \left(\frac{G}{y} - \frac{F}{x} \right) + \frac{\delta xy}{F^2} (1 + GF^{-1}) \left(\frac{G}{y} - \frac{F}{\delta x} \right) \\
 &= \left(\frac{g}{f^2} + \frac{xy(s_h^B y + \beta s_h^A gF^{-1}x)}{(x+y)^2 F^2} \right) \left(\frac{G}{y} - \frac{F}{x} \right) - \frac{\delta xy}{F^2} (1 + GF^{-1}) \left(\frac{\tilde{l}(x,y)}{\delta(x+y)} \right).
 \end{aligned}
 \tag{40}$$

When $\delta > 1$, since $\tilde{l}(x,y) > 0$ and $F > 0$ in \tilde{D}_{11} , we have

$$\frac{G}{y} - \frac{F}{x} < \frac{F}{y} - \frac{1}{\delta} \frac{F}{x} = -\frac{\tilde{l}(x,y)}{\delta(x+y)} < 0.
 \tag{41}$$

With the help of (40) and (41), we have proven that $d^2y/dx^2 < 0$, and hence the solution of (9) is concave-down in \tilde{D}_{11} which is impossible. Therefore, we have proven that the heteroclinic orbit connecting \tilde{E}_0 and \tilde{E}^* must lie entirely in \tilde{D}_{12} .

To get an estimation of the upper bound of $\tilde{h}(x)$, we revisit (23) to get

$$z'(t) = \frac{x'}{\delta x} - \frac{y'}{y} = \frac{\kappa_2 x - \kappa_1 y}{\delta(x+y)} = \frac{\tilde{l}(x,y)}{\delta(x+y)} < 0.$$

Therefore, $z(t)$ decreases monotonically with t in \tilde{D}_{12} , and then

$$x^{1/\delta} \tilde{h}(x)^{-1} > (\tilde{x}^*)^{1/\delta} (\tilde{y}^*)^{-1} \text{ or } \tilde{h}(x) < \tilde{y}^* (x/\tilde{x}^*)^{1/\delta}, \quad 0 < x < \tilde{x}^*.$$

By substituting \tilde{x}^* and \tilde{y}^* into the last inequality, we get

$$\tilde{h}(x) < \frac{\beta \kappa_2 c}{(\kappa_1 + \kappa_2)^2} \left(\frac{(\kappa_1 + \kappa_2)^2 x}{\beta \kappa_1 c} \right)^{1/\delta} = \tilde{h}_1(x), \quad 0 < x < \tilde{x}^*,
 \tag{42}$$

verifying the first part of (37).

Regarding the second part of (37), we notice that the direction vector of $\tilde{\mathcal{L}}$ is not an eigenvector of $\mathcal{J}(\tilde{E}^*)$ for $\delta > 1$, and hence $\tilde{\mathcal{L}}$ is not tangential to the stable curve $\tilde{h}(x)$ at \tilde{E}^* . This implies that the stable curve lies in \tilde{D}_{31} when $x > \tilde{x}^*$ with x being sufficiently close to \tilde{x}^* . Actually, the stable curve will always stay in \tilde{D}_{31} for all $x > \tilde{x}^*$. To see this, we recall (39) and find that all trajectories initiated at $\tilde{\mathcal{L}}$ with $y > \tilde{y}^*$ move into \tilde{D}_{32} when t increases from $t = 0$. Hence, $\tilde{h}(x)$ cannot meet $\tilde{\mathcal{L}}$ from the domain \tilde{D}_{31} when x increases, or equivalently, when t decreases. As $\tilde{l}(x,y) > 0$ in \tilde{D}_{31} , $z(t)$ increases strictly along $\tilde{h}(x)$ in this domain, giving $z(t) < \lim_{t \rightarrow \infty} z(t)$. By the same calculation of deriving (42), we obtain the estimate

$$\tilde{h}(x) > \tilde{h}_1(x), \quad x > \tilde{x}^*,
 \tag{43}$$

completing the proof of (37). The proof of (38) for the case $\delta < 1$ is similar, and we omit it here. This completes the proof. \square

4. Conclusions and Discussion

As one of the most rapidly spreading mosquito-borne infectious diseases, dengue threatens the health of more than half of the global population. In Guangdong Province, China, there was an unprecedented outbreak of dengue in 2014, which reported more cases than the total number in the last decade. Currently, there are no safe and effective specific drugs and vaccines for dengue. Thus, the primary method of prevention and control is to eliminate dengue vectors, including *Aedes albopictus* and *Aedes aegypti*. The direct method to

kill them is spraying insecticides, which is unsustainable because of insecticide resistance, high cost, and environmental pollution. In recent years, scientists have discovered a novel microbial pesticide involving the maternally transmitted endosymbiotic bacteria *Wolbachia*. By inducing cytoplasmic incompatibility (CI), *Wolbachia*-infected males that cause CI have been proposed as an ovicide. Furthermore, *Wolbachia* can block dengue replication in mosquitoes, implying that *Wolbachia* vaccinates female mosquitoes. With these mechanisms, the *Wolbachia* release has been implemented in field experiments in 24 countries worldwide. *Wolbachia* release has been carried out in two different strategies, including population suppression and population replacement. Population suppression requires the inundative releases of *Wolbachia* males to guarantee the effective incompatible matings between wild females and released males. In contrast, population replacement is an inoculated release strategy, which releases both *Wolbachia* males and females to drive the pathogen-blocking trait into the population.

Although various mathematical models for population suppression and population replacement have been developed [17–19,21,40–42,48,49], the model involving bidirectional CI is rarely studied in the previous study. As important as unidirectional CI, bidirectional CI has been frequently reported [28–31]. In addition, the transmission rate and CI intensity are affected by temperature and possibly other environmental conditions [32], which can induce the overlapping of different *Wolbachia* strains in population replacement strategy. Motivated by these considerations, we developed Model (9) to study the global dynamics for competition between two *Wolbachia* strains with bidirectional CI. Our theoretical results provide sharp separatrices determining the competition outcome of the two *Wolbachia* strains. The results help choose appropriate *Wolbachia* strains and design optimal release strategies.

The theoretical results are offered in Sections 3.1 and 3.2. Section 3.1 is focused on the case with complete CI. Theorem 1 shows that System (9) always generates four equilibria, among which the trivial equilibrium E_0 is a source, the two boundary equilibria E_1 and E_2 are sinks, and the unique interior equilibrium E^* is a saddle. To characterize the competition outcome of the two *Wolbachia* strains, Theorem 2 offers a relatively sharp estimation of the stable curve of E^* , above which w -B wins, and below which w -A wins. The stable curves of E^* are located with two analytical functions $h_0(x)$ and $h_1(x)$ defined in Theorem 2. Thus, the global dynamics of System (9) can be totally determined by the stable curve.

To explore the result numerically, we take two *Wolbachia* strains, the benign w Mel [13] and the virulent w MelPop [50] established in *Aedes aegypti*, as an example. Compared to wild *Aedes aegypti*, the w Mel strain did not show significant reductions in fecundity and the egg hatch rate, together with a minor reduction in the mean longevity of adult mosquitoes. In contrast, the virulent w MelPop strain induced strong fitness cost and greatly reduced the fecundity and the egg hatch rate. Moreover, the w MelPop strain caused an approximately 40% reduction in mean longevity. In such a situation, we treat w Mel and w MelPop as the best and the worst *Wolbachia* strains to estimate the range of β and δ in System (9). Recalling that in [21], we estimated the birth rate constants and the death rate constants for w Mel and w MelPop, and obtained

$$w\text{Mel} : b_{w\text{Mel}} = 0.3976, d_{w\text{Mel}} = 9.4482 \times 10^{-6}.$$

$$w\text{MelPop} : b_{w\text{MelPop}} = 0.2154, d_{w\text{MelPop}} = 1.4172 \times 10^{-5}.$$

See Section 4.1 of [21] for a detailed conversion of these parameters based on the experimental data in [13,50]. This leads to

$$\beta \in \left[\frac{0.2154}{0.3976}, \frac{0.3976}{0.2154} \right] = [0.5418, 1.8459], \tag{44}$$

$$\delta \in \left[\frac{9.4482 \times 10^{-6}}{1.4172 \times 10^{-5}}, \frac{1.4172 \times 10^{-5}}{9.4482 \times 10^{-6}} \right] = [0.6667, 1.50]. \tag{45}$$

In the following numerical simulations, we take two parameter combinations with

$$(i) : \beta = 1.2, \delta = 0.8. \quad (ii) : \beta = 0.8, \delta = 1.2,$$

such that β and δ lie in the intervals in (44) and (45), respectively. We first let $s_h^A = s_h^B = 1$, and for case (i) and case (ii) we choose 11 points $x(0) \in [0, 0.5]$, and find $(x(0), y^*)$, such that the solution initiated from $(x(0), y^*)$ of (10) tends to E_1 , while the solution initiated from $(x(0), y^* + 0.0001)$ tends to E_2 . If so, we claim that the point $(x(0), y^*) \in (x, h(x))$. The stable curves of E^* are approximately plotted by seeking 11 points (red stars). In both cases, the stable curves of E^* are sandwiched between $h_0(x)$ and $h_1(x)$ as shown in Figure 5, verifying the estimations of the stable curve shown in Theorem 2.

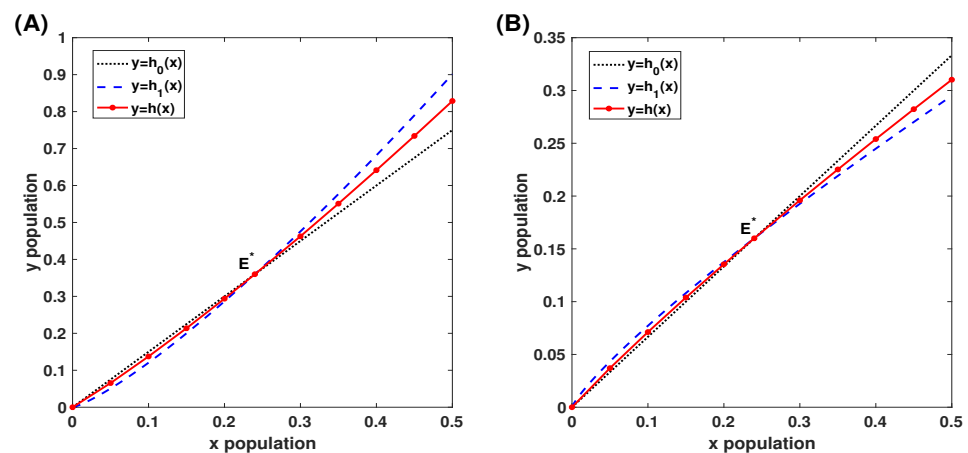


Figure 5. For complete CI with $s_h^A = s_h^B = 1$, panel (A) is for the case with $\beta = 1.2$ and $\delta = 0.8$, and panel (B) is for the case with $\beta = 0.8$ and $\delta = 1.2$.

Regarding the situation with incomplete CI, the dynamics become much more complex. When $\beta = \delta$, the dynamics of System (9) show the same pattern as that of System (8) with complete CI. However, when $\beta \neq \delta$, the existence and stability of equilibria of System (9) depend on the other two thresholds on the CI intensity, denoted by s_A^* and s_B^* . See Table 3 for a summary of counting the equilibria of System (9), together with their stability analysis. The global dynamics of System (9) are proven in Theorems 3 and 4. To check these results numerically, we use pplane10 in Matlab to plot dynamics of System (9) when $\beta = 1.2$ and $\delta = 0.8$. This yields $s_A^* = 1/3$. Fix $s_h^B = 0.9$. Panel A in Figure 6 shows that any solutions initiated from the interior of the first quadrant tends to $(1.5, 0)$; that is, w -A outcompetes w -B and dominates the mosquito population. However, when taking $s_h^A = 0.5 > s_A^*$, the saddle point $E^* = (0.13085, 0.73278)$ appears. The stable curves of E^* , shown in black curves in Panel B in Figure 6, determine the outcome of competition results between w -A and w -B strains. Similar figures can be plotted for the case $\beta < \delta$, which we omit here.

It is well known that mosquitoes undergo four metamorphosis stages: egg, larva, pupa, and adult. Our current study only models the dynamics of adult mosquitoes, leaving the first three aquatic stages untouched. To characterize the developmental traits in aquatic stages, we have tried two modeling ideas in our previous works. The first one formulated stage-structured models by using difference equations that include the four stages of mosquitoes to predict the mosquitoes' abundance in [51], together with an exploration of the optimal release strategies specific to *Aedes albopictus* in Guangzhou [52]. The second assumed that the average waiting time from mating to the emergence of reproductive progenies is kept as a constant τ and studied the interactive dynamics of *Wolbachia*-infected and wild mosquitoes [17–20,53]. To see the impact of aquatic stages on the competition between two *Wolbachia* strains, in our future work, we shall embed the aquatic stages into System (9), either by adding equations for aquatic stages or by introducing the maturation delays.

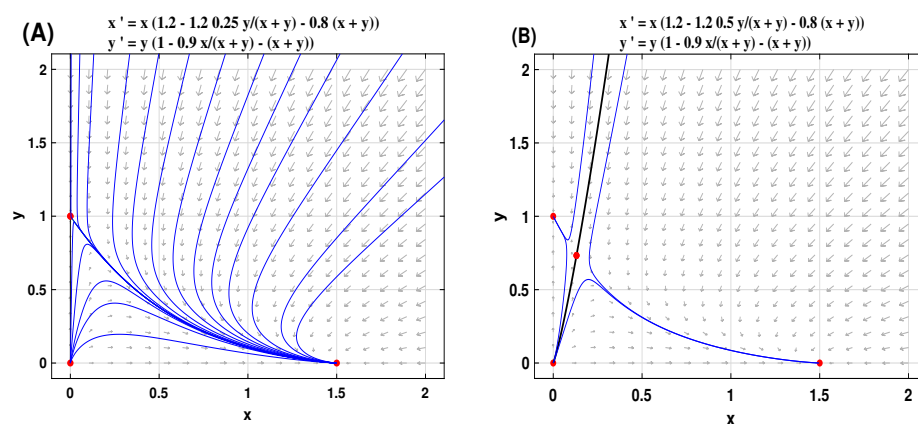


Figure 6. Take $\beta = 1.2$ and $\delta = 0.8$, we get $s_A^* = 1/3$. Fix $s_h^B = 0.9$. Panel (A) is for the case with $s_h^A = 0.25 < s_A^*$, and panel (B) is for the case with $s_h^A = 0.5 > s_A^*$.

Author Contributions: Conceptualization, B.Z.; data curation, L.C.; formal analysis, L.C., Z.Z. and B.Z.; methodology, Q.H.; software, L.C.; supervision, B.Z.; visualization, Z.Z.; writing—original draft, Q.H., Z.Z. and B.Z.; writing—review and editing, Q.H., Z.Z. and B.Z. All authors have read and agreed to the published version of the manuscript.

Funding: This research was funded by the National Natural Science Foundation of China, grant numbers 11971127, 12071095.

Data Availability Statement: Not applicable.

Conflicts of Interest: The authors declare no conflict of interest.

References

1. WHO. Vector-Borne Diseases. 2020. Available online: <https://www.who.int/news-room/fact-sheets/detail/vector-borne-diseases> (accessed on 4 September 2022).
2. Bhatt, S.; Gething, P.W.; Brady, O.J.; Messina, J.P.; Farlow, A.W. The global distribution and burden of dengue. *Nature* **2013**, *496*, 504–507. [[CrossRef](#)] [[PubMed](#)]
3. Brady, O.J.; Gething, P.W.; Bhatt, S.; Messina, J.P.; Brownstein, J.S.; Hoen, A.G.G.; Moyes, C.L.; Farlow, A.W.; Scott, T.W.; Hay, S.I. Refining the global spatial limits of dengue virus transmission by evidence-based consensus. *PLoS Negl. Trop. Dis.* **2012**, *6*, e1760. [[CrossRef](#)] [[PubMed](#)]
4. Zoh, M.G.; Gaude, T.; Prudhomme, S.M.; Riaz, M.A.; David, J.P.; Reynaud, S. Molecular bases of P450-mediated resistance to the neonicotinoid insecticide imidacloprid in the mosquito *Ae. aegypti*. *Aq. Toxicol.* **2021**, *236*, 105860. [[CrossRef](#)]
5. Fatima, A. Dengue vaccine fiasco leads to criminal charges for researcher in the Philippines. *Science* **2019**, *364*, 6438.
6. Jon, C. Dengue may bring out the worst in Zika. *Science* **2017**, *356*, 175–180.
7. Hilgenboecker, K.; Hammerstein, P.; Schlattmann, P.; Telschow, A.; Werren, J.H. How many species are infected with *Wolbachia*? A statistical analysis of current data. *FEMS Microbiol. Lett.* **2008**, *281*, 215–220. [[CrossRef](#)]
8. Hertig, M.; Wolbach, S.B. Studies on rickettsia-like microorganisms in insects. *J. Med. Res.* **1924**, *44*, 329–374.
9. Ghelelovitch, S. Genetic determinism of sterility in the cross-breeding of various strains of *Culex autogenicus* Roubaud. *C. R. Hebd. Seances Acad. Sci.* **1952**, *234*, 2386–2388.
10. Xi, Z.; Khoo, C.C.H.; Dobson, S.L. *Wolbachia* establishment and invasion in an *Aedes aegypti* laboratory population. *Science* **2005**, *310*, 326–328. [[CrossRef](#)] [[PubMed](#)]
11. Xi, Z.; Khoo, C.C.H.; Dobson, S.L. Interspecific transfer of *Wolbachia* into the mosquito disease vector *Aedes albopictus*. *Proc. Biol. Sci.* **2006**, *273*, 1317–1322.
12. Zheng, B.; Yu, J.; Li, J. Modeling and analysis of the implementation of the *Wolbachia* incompatible and sterile insect technique for mosquito population suppression. *SIAM J. Appl. Math.* **2021**, *81*, 718–740. [[CrossRef](#)]
13. Walker, T.; Johnson, P.H.; Moreira, L.A.; Iturbe-Ormaetxe, I.; Frentiu, F.D.; McMeniman, C.J.; Leong, Y.S.; Dong, J.; Axford, J.; Kriesner, P.; et al. The *wMel* *Wolbachia* strain blocks dengue and invades caged *Aedes aegypti* populations. *Nature* **2011**, *476*, 450–453. [[CrossRef](#)] [[PubMed](#)]
14. Hoffmann, A.A.; Montgomery, B.L.; Popovici, J.; Iturbe-Ormaetxe, I.; Johnson, P.H.; Muzzi, F. Successful establishment of *Wolbachia* in *Aedes* populations to suppress dengue transmission. *Nature* **2011**, *476*, 450–455. [[CrossRef](#)] [[PubMed](#)]

15. Ryan, P.A.; Turley, A.P.; Wilson, G.; Hurst, T.P.; Retzki, K.; Brown-Kenyon, J.; Hodgson, L.; Kenny, N.; Cook, H.; Montgomery, B.L.; et al. Establishment of *wMel* *Wolbachia* in *Aedes aegypti* mosquitoes and reduction of local dengue transmission in Cairns and surrounding locations in northern Queensland. *Gates Open Res.* **2020**, *3*, 1547. [[CrossRef](#)] [[PubMed](#)]
16. Powell, J.R. Modifying mosquitoes to suppress disease transmission: Is the long wait over? *Genetics* **2022**, *221*, 3. [[CrossRef](#)]
17. Yu, J. Existence and stability of a unique and exact two periodic orbits for an interactive wild and sterile mosquito model. *J. Differ. Equ.* **2020**, *269*, 10395–10415. [[CrossRef](#)]
18. Yu, J.; Li, J. A delay suppression model with sterile mosquitoes release period equal to wild larvae maturation period. *J. Math. Biol.* **2022**, *84*, 14. [[CrossRef](#)]
19. Zheng, B. Impact of releasing period and magnitude on mosquito population in a sterile release model with delay. *J. Math. Biol.* **2022**, *85*, 18. [[CrossRef](#)]
20. Zheng, B.; Li, J.; Yu, J. Existence and stability of periodic solutions in a mosquito population suppression model with time delay. *J. Differ. Equ.* **2022**, *315*, 159–178. [[CrossRef](#)]
21. Zheng, B.; Tang, M.; Yu, J. Modeling *Wolbachia* spread in mosquitoes through delay differential equation. *SIAM J. Appl. Math.* **2014**, *74*, 743–770. [[CrossRef](#)]
22. Hu, L.; Huang, M.; Tang, M.; Yu, J.; Zheng, B. *Wolbachia* spread dynamics in stochastic environments. *Theor. Popul. Biol.* **2015**, *106*, 32–44. [[CrossRef](#)]
23. Huang, M.; Tang, M.; Yu, J. *Wolbachia* infection dynamics by reaction-diffusion equations. *Sci. China Math.* **2015**, *58*, 77–96. [[CrossRef](#)]
24. Huang, M.; Hu, L.; Yu, J.; Zheng, B. Qualitative analysis for a *Wolbachia* infection model with diffusion. *Sci. China Math.* **2016**, *59*, 1249–1266. [[CrossRef](#)]
25. Breeuwer, J.A.J.; Werren, J.H. Microorganisms associated with chromosome destruction and reproductive isolation between two insect species. *Nature* **1990**, *346*, 558–560. [[CrossRef](#)]
26. O'Neill, S.L.; Karr, T.L. Bidirectional incompatibility between conspecific populations of *Drosophila simulans*. *Nature* **1990**, *348*, 178–180. [[CrossRef](#)]
27. Werren, J.H.; Baldo, L.; Clark, M.E. *Wolbachia*: Master manipulators of invertebrate biology. *Nat. Rev. Microbiol.* **2008**, *6*, 714–751. [[CrossRef](#)] [[PubMed](#)]
28. Calvitti, M.; Moretti, R.; Skidmore, A.R.; Dobson, S.L. *Wolbachia* strain *wPip* yields a pattern of cytoplasmic incompatibility enhancing a *Wolbachia*-based suppression strategy against the disease vector *Aedes albopictus*. *Parasite Vectors* **2012**, *5*, 254. [[CrossRef](#)] [[PubMed](#)]
29. Ant, T.H.; Herd, C.; Louis, F.; Failloux, A.B.; Sinkins, S.P. *Wolbachia* transinfections in *Culex quinquefasciatus* generate cytoplasmic incompatibility. *Insect Mol. Biol.* **2020**, *29*, 1–8. [[CrossRef](#)]
30. Sicard, M.; Bouchon, D.; Ceyrac, L.; Raimond, R.; Thierry, M.; Clec'h, L.W. Bidirectional cytoplasmic incompatibility caused by *Wolbachia* in the terrestrial isopod *Porcellio dilatatus*. *J. Invertebr. Pathol.* **2014**, *121*, 28–36. [[CrossRef](#)]
31. Ant, T.H.; Herd, C.S.; Geoghegan, V.; Hoffmann, A.A.; Sinkins, S.P. The *Wolbachia* strain *wAu* provides highly efficient virus transmission blocking in *Aedes aegypti*. *PLoS Pathog.* **2018**, *14*, e1006815. [[CrossRef](#)]
32. Ross, P.A.; Wiwatanaratnabutr, I.; Axford, J.K.; White, V.L.; Endersby-Harshman, N.M.; Hoffmann, A.A. *Wolbachia* infections in *Aedes aegypti* differ markedly in their response to cyclical heat stress. *PLoS Pathog.* **2016**, *13*, e1006006. [[CrossRef](#)] [[PubMed](#)]
33. Bordenstein, S.R. Temperature affects the tripartite interactions between bacteriophage WO, *Wolbachia*, and cytoplasmic incompatibility. *PLoS ONE* **2011**, *6*, e29106. [[CrossRef](#)] [[PubMed](#)]
34. Feder, M.E.; Karr, T.L.; Yang, W.; Hoekstra, J.M.; James, A.C. Interaction of *Drosophila* and its endosymbiont *Wolbachia*: Natural heat shock and the overcoming of sexual incompatibility. *Am. Zool.* **1999**, *39*, 363–373. [[CrossRef](#)]
35. Wiwatanaratnabutr, I.; Kittayapong, P. Effects of crowding and temperature on *Wolbachia* infection density among life cycle stages of *Aedes albopictus*. *J. Invertebr. Pathol.* **2009**, *102*, 220–224. [[CrossRef](#)]
36. Turelli, M. Cytoplasmic incompatibility in populations with overlapping generations. *Evolution* **2010**, *64*, 232–241. [[CrossRef](#)]
37. Turelli, M.; Hoffmann, A.A. Rapid spread of an inherited incompatibility factor in California *Drosophila*. *Nature* **1991**, *353*, 440–442. [[CrossRef](#)]
38. Caspari, E.; Watson, G.S. On the evolutionary importance of cytoplasmic sterility in mosquitoes. *Evolution* **1959**, *13*, 568–570. [[CrossRef](#)]
39. Aida, H.N.; Dieng, H.; Nurita, A.T.; Salmah, M.C.; Miake, F.; Norasmah, B. The biology and demographic parameters of *Aedes albopictus* in northern peninsular Malaysia. *Asian Pac. J. Trop. Biomed.* **2011**, *1*, 472–477. [[CrossRef](#)]
40. Keeling, M.J.; Jiggins, F.M.; Read, J.M. The invasion and coexistence of competing *Wolbachia* strains. *Heredity* **2003**, *90*, 220–226. [[CrossRef](#)]
41. Zheng, B.; Li, J.; Yu, J. One discrete dynamical model on *Wolbachia* infection frequency in mosquito populations. *Sci. China Math.* **2022**, *65*, 1749–1764. [[CrossRef](#)]
42. Zheng, B.; Yu, J. Existence and uniqueness of periodic orbits in a discrete model on *Wolbachia* infection frequency. *Adv. Nonlinear Anal.* **2022**, *11*, 212–224. [[CrossRef](#)]
43. McMeniman, C.J.; Lane, R.V.; Cass, B.N.; Fong, A.W.C.; Sidhu, M.; Wang, Y.F.; O'Neill, S.L. Stable Introduction of a Life-Shortening *Wolbachia* Infection into the Mosquito *Aedes aegypti*. *Science* **2009**, *323*, 141–144. [[CrossRef](#)] [[PubMed](#)]

44. Calvitti, M.; Moretti, R.; Lampazzi, E.; Bellini, R.; Dobson, S.L. Characterization of a New *Aedes albopictus* (Diptera: Culicidae)-*Wolbachia pipientis* (Rickettsiales: Rickettsiaceae) Symbiotic Association Generated by Artificial Transfer of the *wPip* Strain from *Culex pipiens* (Diptera: Culicidae). *J. Med. Entomol.* **2010**, *47*, 179–187. [[CrossRef](#)]
45. Hirsch, M.W.; Smale, S.; Devaney, R.L. *Differential Equations, Dynamical Systems, and an Introduction to Chaos*, 2nd ed.; Elsevier: New York, NY, USA, 2004; pp. 166–174.
46. Adams, K.L.; Abernathy, D.G.; Willett, B.C.; Selland, E.K.; Itoe, M.A.; Catteruccia, F. *Wolbachia cifB* induces cytoplasmic incompatibility in the malaria mosquito vector. *Nat. Microbiol.* **2021**, *6*, 11575–11582. [[CrossRef](#)] [[PubMed](#)]
47. Pinto, S.B.; Stainton, K.; Harris, S.; Kambris, Z.; Sutton, E.R.; Bonsall, M.B.; Parkhill, J.; Sinkins, S.P. Transcriptional regulation of *Culex pipiens* mosquitoes by *Wolbachia* influences cytoplasmic incompatibility. *PLoS Pathog.* **2013**, *9*, e1003647. [[CrossRef](#)]
48. Cai, L.; Ai, S.; Fan, G. Dynamics of delayed mosquitoes populations model with two different strategies of releasing sterile mosquitoes. *Math. Biosci. Eng.* **2008**, *15*, 1181–1202. [[CrossRef](#)]
49. Zheng, X.; Zhang, D.; Li, Y.; Yang, Y.; Wu, Y.; Liang, X.; Liang, Y.; Pan, X.; Hu, L.; Sun, Q.; et al. Incompatible and sterile insect techniques combined eliminate mosquitoes. *Nature* **2019**, *572*, 56–61. [[CrossRef](#)]
50. Yeap, H.L.; Mee, P.; Walker, T.; Weeks, A.R.; O’Neill, S.L.; Johnson, P.; Ritchie, S.A.; Richardson, K.M.; Doig, C.; Endersby, N.M.; et al. Dynamics of the “popcorn” *Wolbachia* infection in outbred *Aedes aegypti* informs prospects for mosquito vector control. *Genetics* **2011**, *187*, 583–595. [[CrossRef](#)]
51. Zheng, B.; Yu, J.; Xi, Z.; Tang, M. The annual abundance of dengue and Zika vector *Aedes albopictus* and its stubbornness to suppression. *Ecol. Model.* **2018**, *387*, 38–48. [[CrossRef](#)]
52. Zheng, B.; Liu, X.; Tang, M.; Xi, Z.; Yu, J. Use of age-stage structural models to seek optimal *Wolbachia*-infected male mosquito releases for mosquito-borne disease control. *J. Theor. Biol.* **2019**, *472*, 95–109. [[CrossRef](#)]
53. Yu, J.; Li, J. Global asymptotic stability in an interactive wild and sterile mosquito model. *J. Differ. Equ.* **2020**, *269*, 6193–6215. [[CrossRef](#)]

Disclaimer/Publisher’s Note: The statements, opinions and data contained in all publications are solely those of the individual author(s) and contributor(s) and not of MDPI and/or the editor(s). MDPI and/or the editor(s) disclaim responsibility for any injury to people or property resulting from any ideas, methods, instructions or products referred to in the content.